

Reduction of Residual Generated by Vibration Actuator Type Motor Step in a Flexible Beam Euler-Bernoulli

WANTUIR AP. FREITAS¹, ANDRÉ FENILI², MÁRIO CÉSAR RICCI¹

1 – National Institute for Space Research / Division of Space Mechanics and Control
Av. dos Astronautas, 1758, Jardim da Granja, São José dos Campos – SP/Brasil

2 – Federal University of ABC
Center for Engineering, Modeling and Applied Social Sciences (CECS)
Aerospace Engineering
Av. dos Estados, 5001, Bairro Bangu, Santo André – SP/Brasil
wantuir@hotmail.com, andre.fenili@ufabc.edu.br, mcr@dem.inpe.br

Abstract: - The technique for formatting the input shaping, based on the pole-zero cancellation is used to reduce the residual vibration in a flexible structure. The technique is developed in the discrete time domain and was extended for a step motor actuator where the motor drive commands were modified to act as passive control. The mathematical model is represented by a central body, wings of rigid solar panels and a flexible beam as shown in Figure 1. The methodology of the system analyze was developed as a multi-body problem in Cartesian plane. The external torque which acts on the structure was generated by stepper motor actuators, whose step numbers were variable in order to cause an effect on the structure and minimize the linear structural response on the flexible beam Two passive control strategies to minimize the vibration of the flexible beam first vibration mode, were investigated. The first strategy allocates a zero on the pole of the system and the second considers uncertainties on the system parameters and two zeros were placed near the pole.

Key Words: - stepper motor, digital control, pole-zero, vibration, normal modes, input shapers

1 Introduction

Artificial satellites in operation need to develop certain functions precisely as attitude and orbit control, telecommunications, among other maneuvers, such as pointing cameras are necessary to obtain high-resolution images. To meet the requirements of the mission and well-functioning of the subsystems, the performance of a satellite depends on the power source (battery) which feeds the equipment on board. Therefore, the solar panels need maximize the energy capture, being their pointing towards the Sun regularly adjusted. The wing panels incorporate an electromechanical mechanism that transmits electrical signals and power into the satellite. This mechanism is known in the literature as BAPTA (Bearing and Power Transfer Assembly) or SADA (Solar Array Drive Assembly). In this kind of mechanism is one of its elements is a stepper motor which has the function of transmitting the rotational movement to the shaft of the wing panels. The stepper motor drive, can cause unwanted vibrations in the payload, which must be minimized during the performance of operational tasks, sensitive to vibrations. These vibrations can be minimized by controlling the input shaping that governs the number of steps of the motor [1] There are many input shaping methods

using time domain or the frequency domain , has been developed . Singer [14] proposed a method of sequential pulses for vibration control in the continuous time domain, which was later extended by Hyde and Seering [15] to include the elimination of multiple vibration modes . Murphy and Watanabe [16] and Singh and Vadali [17] showed that work with the input shaping technique in the Laplace s-plane or z-plane of the discrete time , instead of working in the continuous time domain, provides significant gains in mathematical simplicity , especially when a systems with multiple unwanted modes of vibration. Tuttle and Seering [1] proposed a formulation for designing a technique based on the input shaping technique of Singer, but using the pole-zero cancellation in discrete-time domain , suggested by Smith [18] . In this work , is used the technique of placing zeros in the development of an input shaping algorithm of the entry, which must meet the requirements of the dynamic vibration system , obeying the operational capability of a stepper motor actuator type . Therefore, it is an extension of the work Tuttle Seering and the dynamics of the stepper motor. The pulse-width modulation driver is an excellent driver which offers good current build-up with low loss [12].

2 Determination of the vibration target modes

The study of vibrations is related to the analysis of the oscillatory behavior of an elastic body and the forces and / or momentum associated. The vibrations can be classified as: free vibrations and forced vibrations . When a system oscillates due to the action of a non-zero initial condition (position and / or velocity) and no force and / or external momentum acting on the system , it says that the system oscillates freely. In this case, depending on which mode the system is more excited , characterized by the nature of the material, the distribution of mass and stiffness. The forced vibration arises due to the action of forces and / or external momentum when the natural frequency of external excitation coincides with one of natural frequencies of the system. The kinetic energy of the system increases until it reaches a resonance state. Therefore, the calculation of natural frequencies is of fundamental importance when it comes to vibration control of flexible structures . In this paper for the design of vibration structural control induced by a stepper motor, an experimental model was constructed of aluminum alloy . The aluminum alloy is the most widely used material in the construction of satellites, due its relatively lightweight, sturdy, easy to machine and low cost [7,13]. The project of a structure involves the calculation of its natural frequencies. Complex structures are simulated by a numerical model, as the one created with finite elements, to obtain more accurate values of the natural frequencies. To determine the vibration modes that the input torque generated by the stepper motor with the payload (flexible beam), more strongly a frequency response analysis is performed. At the free end of the flexible beam, an accelerometer is installed to collect the acceleration data generated due to drive the stepper motor when performing a maneuver of angular displacement. The acceleration data are stored in a digital computer to be converted into displacement data for analysis and comparison with theoretical data. Table 1 summarizes the dimensions of the mass, geometry and corresponding moments of inertia of the experimental model.

Table 1: Dimensions, mass, geometry and momentum of inertia.

	Dimension (m)	Mass (kg)	I_{xx} Nms ²	I_{yy} Nms ²	I_{zz} Nms ²
CS	.31x.31x.31	4.219	.086	.055	.094
SAW	.33x.6x.01	.708	.030	.037	3.06e-4
FB	.015x.0005x1.2	1.6e-4	1.9e-5	2.5e-8	1.9e-5

SB = Satellite Body, SAW=Solar Array Wing
FB=Flexible Beam

Lagrangian formalism is used to obtain the governing equations of motion. The flexible beam is modeled as a Euler-Bernoulli cantilever beam and using the linear theory of bending. Only the first bending mode is considered and the behavior of the beam is observed during and after the actuator drive stepper motor. Two control strategies are investigated. The rate of steps per second in both cases is fifty paces per second.

3 Frequency Response Function

The frequency response function (FRF) defines quantitatively the relationship between external excitation input and a position that we want to evaluate, as the output position in a structure, for a range of frequencies. The input is a SADA node torque in the Z-direction and the output is a translation in the X-direction of the node located at the free end of the flexible beam. For a modal system with two degrees of freedom, the Frequency Response Function [2], is:

$$H_{ij}(\omega) = \sum_{r=1}^N \frac{\phi_{ij}\phi_{jr} / m_r}{(\omega_{nr}^2 - \omega^2) + j2\xi_r\omega_{nr}\omega} \quad (1)$$

where there are N modes to be included. The r-th mode has natural frequency ω_{nr} , damping ratio ξ_r , modal mass m_r and ϕ_{ij} e ϕ_{jr} being the mode shape coefficients (i for the input mode and j to the output mode). $H_{ij}(\omega)$ is a complex number and is showed on a magnitude and phase graph [4]. The values obtained by the frequency response function are classified and used to identify the most important modes.

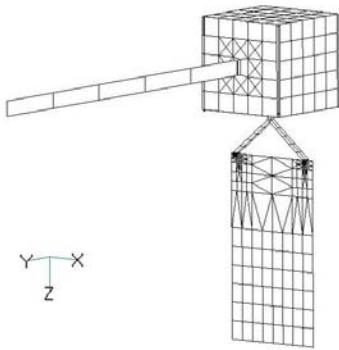


Figure 1: Finite Element Model of the studied system

3.1 Frequency Response Analysis

Figures 2, 3 and 4 show the frequency response function analysis, with the torque stepper motor as the input and the translation of the beam as the output. The response frequency of the beam end on Y-axis and Z-axis is practically zero over the entire frequency range corresponding to a low rate of energy transfer from Z-axis to Y-axis. Thus, the analysis of the vibration modes is specified with respect to the X-axis, to the frequency 1,938 Hz which corresponds to the first mode of vibration of the flexible beam, having a high magnitude of response if compared to the whole frequency range.

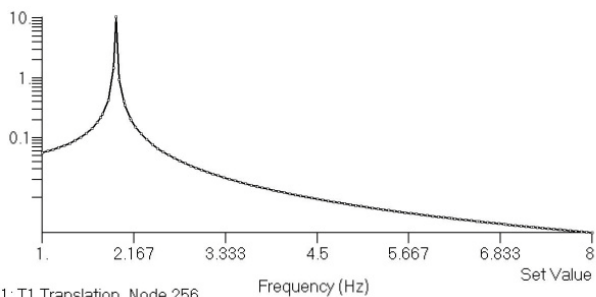


Figure 2 - Frequency response function with translation in X-axis.

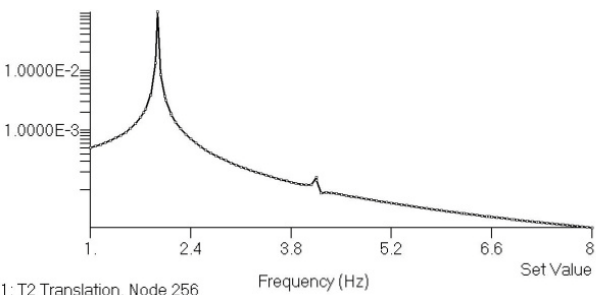


Figure 3 - Frequency response function with translation in Y-axis.

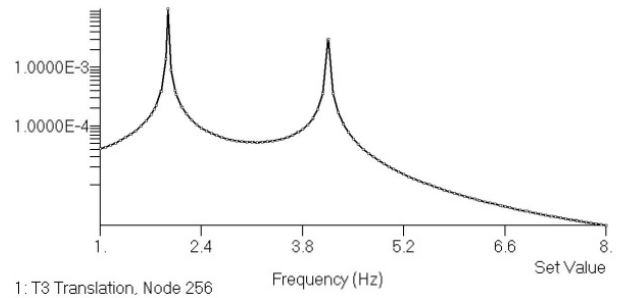


Figure 4 - Frequency response function with translation in Z-axis.

4 Selection of Target Modes

Figure 2 summarizes the results of the FRF analysis indicating the dominant mode of vibration in the behavior of the flexible beam due to the application of a torque unit as an input. The largest contribution to the translation along the X-axis is the mode number 7 which corresponds to the first flexible mode of vibration system. This mode is chosen as the target mode to input shaping of the stepper motor in order to neutralize the first flexible mode of the beam in the X-axis. To neutralize or reduce residual vibrations to acceptable levels, the shaper must have zeros on or near the poles unwanted dynamical system. The poles in the discrete domain are defined by complex conjugate pairs

$$\begin{aligned}
 p_i &= e^{-\zeta_i \omega_{ni} T} e^{j \omega_{di} T} \\
 p_i^* &= e^{-\zeta_i \omega_{ni} T} e^{-j \omega_{di} T}
 \end{aligned}
 \tag{2}$$

where T is the discrete sampling period, ω_{ni} are the natural frequencies, ζ is damping ratio of the modes, ω_{di} is the damped natural frequencies of the modes and $i = 1, 2$ and 3 ,

$$\omega_{di} = \sqrt{1 - \zeta^2}
 \tag{3}$$

5 Control strategy

Can be obtained from an infinite number of transfer functions for the input shaper. However, the shaper should be able to:

- eliminate unwanted vibration modes of the system,
- provide robustness due to the uncertainties of the system,
- must consider the effect of causality,
- the need to minimize distortions on the input command,
- the shaper commands cannot exceed the limits of the stepper motor.

Once the the vibration flexible mode was rated with a frequency 1,938 Hz, two strategies of command sequence for the stepper motor were developed [9-11]. In the first strategy one zero was allocate on the pole of the system. The second control strategy, considers the uncertainties in the system parameters and two zeros were allocated near the pole. Nothing stops you from using parameter identification techniques [5,8]. For the natural frequency found and the damping ratio of 0.2%, the pole in the Z-plane can be calculated directly from equation 2 [1],

$$\begin{aligned} \rho_3 &= R_3 e^{+j\chi_3}, \text{ where } R_1 = e^{-\xi\omega_{n3}T}, \chi_1 = \omega_{d3}T \\ \rho_3^* &= R_3 e^{-j\chi_3}, \text{ where } R_1 = e^{-\xi\omega_{n3}T}, \chi_1 = \omega_{d3}T \end{aligned} \quad (4)$$

$$\begin{aligned} \rho_1 &= R_1 e^{+j\chi_1}, \text{ where } R_1 = e^{-\xi\omega_{n1}T}, \chi_1 = \omega_{d1}T \\ \rho_1^* &= R_1 e^{-j\chi_1}, \text{ where } R_1 = e^{-\xi\omega_{n1}T}, \chi_1 = \omega_{d1}T \\ \rho_2 &= R_2 e^{+j\chi_2}, \text{ where } R_2 = e^{-\xi\omega_{n2}T}, \chi_2 = \omega_{d2}T \\ \rho_2^* &= R_2 e^{-j\chi_2}, \text{ where } R_2 = e^{-\xi\omega_{n2}T}, \chi_2 = \omega_{d2}T \end{aligned} \quad (5)$$

The graph pole-zero of the system for the first control strategy is shown in Figure 5 for a sampling period $T = 0.1718$ seconds obtained from the analysis of the Figure 7.

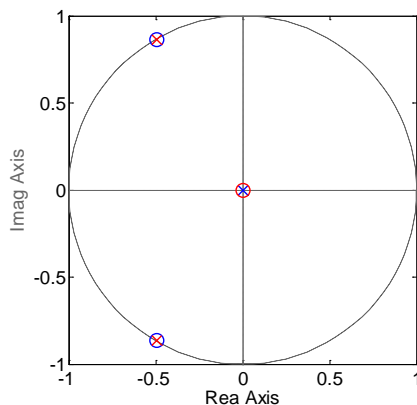


Figure 5 - Pole and zero in the Z-plane: first control strategy

The second control strategy considers variations or inaccuracies in the system parameters. Two zeros at frequencies $f_1 = 1,934$ Hz and $f_2 = 1,942$ Hz, are allocated near the pole frequency $f_3 = 1,938$ Hz as shown in Figure 6. The sampling period is now $T = 0.129$ seconds obtained from the analysis of the impulsive amplitudes plots, Figure 9. The pole in the Z-plane is calculated directly from equation (3).

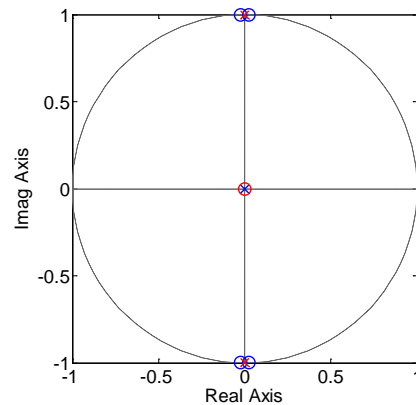


Figure 6 - Pole and zero in Z-plane second control strategy

6 Shaper Design Techniques to the First Control Strategy

The shaper transfer function containing the poles and the zero at the origin of the z-plane for the first control strategy is:

$$H(z) = C \frac{(z-\rho_1)(z-\rho_1^*)}{z^2} \quad (6)$$

where C is a normalization constant.

Substituting the equation (4) into (6) and multiplying the numerator, the shaper transfer function takes the form:

$$H(z) = C \frac{z^2 + a_1z + a_2}{z^2} \quad (7)$$

where a_i is called impulsive amplitude. Using the trigonometric identity $2 \cos(\chi) = e^{j\chi} + e^{-j\chi}$ the expressions for a_1 and a_2 takes the form:

$$a_1 = 2R_1 \cos(\chi) \text{ e } a_2 = R_1^2 \quad (8)$$

The transfer function, equation (7), is mapped from z-plane into the s-plane by the relation

$$z = e^{sT} \quad (9)$$

Thus,

$$H(z) = C \frac{e^{2sT} + a_1 e^{sT} + a_2}{e^{2sT}} \quad (10)$$

Dividing the numerator by the denominator of equation the (10) and applying the inverse Laplace Transform, the transfer function in the time domain is obtained.

$$h(t) = C[\delta(t) + a_1\delta(t-T) + a_2\delta(t-2T)] \quad (11)$$

7 Impulse Amplitudes as a Function of Time and Selection of the Sampling Period T.

In Figure 7 each impulse amplitude is calculated from equation (8) to a_i with $i = 1$ and 2. The sampling period is determined from the graph of impulsive amplitude. Analysis of Figure 7 shows that the value of T which all amplitudes are positive is $T = 0.1718$ seconds.

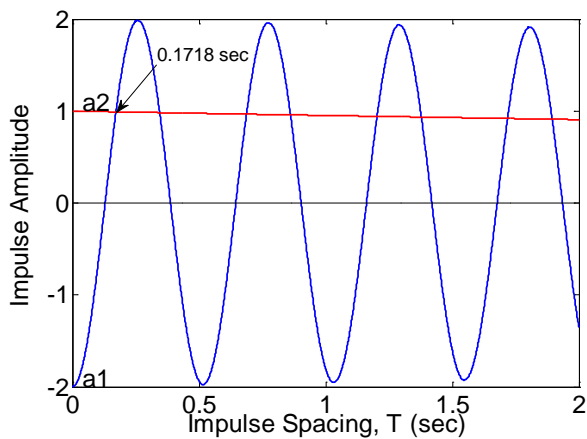


Figure 7: Function amplitude, first control strategy

Impulsive amplitudes are determined for the value of the sampling period founded. The constant C is used to normalize the sum of the amplitudes. Thus, the shaper pulse sequence for the first control strategy to counteract the obtained frequency of 1,983 Hz is:

$$h(t) = 0,33352\delta(t) + 0,33352\delta(t - 0,1718) + 0,33352\delta(t - 0,3436) \quad (12)$$

Figure 8 shows graphically this sequence of impulsive torque.

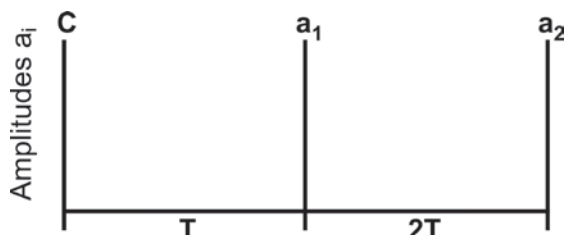


Figure 8: Impulsive Amplitude, first control strategy.

8 Shaper Design Techniques to second control strategy

The second control strategy considers variations or inaccuracies in the system parameters. In this case, two zeros at the frequencies $f_1 = 1,934$ Hz and $f_2 = 1,942$ Hz, are allocated near the pole frequency of $f_3 = 1,938$ Hz, as shown in Figure 6. The sampling period $T = 0.129$ seconds is obtained from the analysis graphic of the impulsive amplitudes, Figure 9.

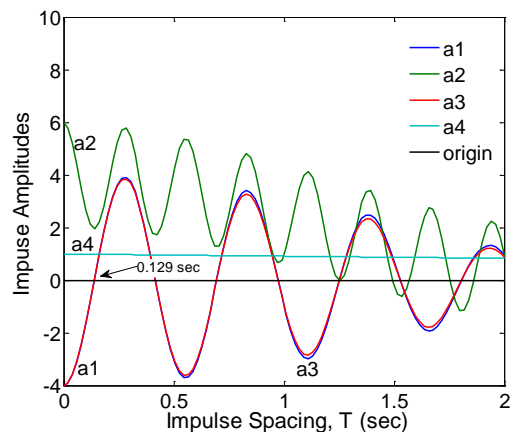


Figure 9: Function amplitude, second control strategy

The zeros of the shaper can be written as:

$$\begin{aligned} p_1 &= R_1 e^{i\chi_1}, \text{ where} \\ R_1 &= e^{0,0039\pi T}, \chi_1 = 3,868\pi T \\ p_1^* &= R_1 e^{-i\chi_1}, \text{ where} \\ R_1 &= e^{-0,0039\pi T}, \chi_1 = 3,868\pi T \\ p_2 &= R_2 e^{i\chi_2}, \text{ where} \\ R_2 &= e^{0,0039\pi T}, \chi_2 = 3,864\pi T \\ p_2^* &= R_2 e^{-i\chi_2}, \text{ where} \\ R_2 &= e^{-0,0039\pi T}, \chi_2 = 3,864\pi T \end{aligned} \quad (13)$$

and the shaper transfer function is:

$$H(z) = C \frac{(z - p_1)(z - p_1^*)(z - p_2)(z - p_2^*)}{z^4} \quad (14)$$

where C is a constant.

Substituting the equation (13) into (14) and multiplying the numerator, the shaper transfer function takes the form:

$$H(z) = C \frac{z^2 + a_1 z^3 + a_2 z^2 + a_3 z + a_4}{z^4} \quad (15)$$

where a_1, a_2, a_3 e a_4 are:

$$\begin{aligned}
 a_1 &= -2(R_1 \cos(\theta_1) + R_2 \cos(\theta_2)) \\
 a_2 &= R_1^2 + 4R_1 R_2 \cos(\theta_1) \cos(\theta_2) + R_2^2 \\
 a_3 &= -2(R_1 R_2^2 \cos(\theta_1) + R_1^2 R_2 \cos(\theta_2)) \\
 a_4 &= R_1^2 R_2^2.
 \end{aligned}
 \tag{16}$$

The transfer function, equation (15), is mapped from the z-plane into the s-plane by the relation

$$z = e^{sT} \tag{17}$$

Dividing the numerator by the denominator of equation (15) and applying inverse Laplace Transform, the transfer function in the time domain is obtained.

$$\begin{aligned}
 h(t) &= 0,2455\delta(t) + 0,4880\delta(t - 0,258) + \\
 &0,2424\delta(t - 0,516)
 \end{aligned}
 \tag{18}$$

Graphically this sequence of impulsive torque is shown in Figure 10.



Figure 10: Impulsive amplitude, second control strategy.

9 Error Calculation

In general the sequence of steps produced by the shaper is not an integer steps, being necessary the rounding to integer values to be implemented in a step motor.

The total error produced by rounding the amplitude is defined as the sum of the magnitudes of the differences between the amplitudes and the rounded amplitudes a_i [4].

$$E_{arred}^{total} = \sum_{i=1}^{2N+1} |a_i - arred(a_i)| \tag{19}$$

10. Theoretical and Experimental Results

The behavior of the flexible beam because the first control strategy in order to minimize the vibration of the flexible beam is shown in Figures 14 and 15. Figure 14 represents the theoretical behavior of the beam, while Figure 15 shows the results obtained experimentally. For the first control strategy, the

stepper motor is driven at each sampling period $T = 0.1718$ seconds. Each period T the motor performs four steps, three periods of sampling for the stepper motor rotate 10.8 degrees is required. When applying the first control strategy the oscillatory behavior of the flexible beam was well below the oscillatory behavior due to the first sequence drive the stepper motor. Experimental data also showed a reduction in oscillatory behavior of the flexible beam, when applying the first control strategy, as illustrated in Figures 16 and 17. The second control strategy considered possible inaccuracies and variations in system parameters due to non-structural mass as bumper nuts and bolts . The second control strategy for residual vibrations , there was a significant reduction in the oscillatory behavior of the flexible beam, compared with the curve of the first sequence of actuation of the stepper motor. The allocation of another zero near the pole of the system , not completely neutralize the influence of the pole , however , meant that the amplitude of the flexible beam decays to lower values compared to the first sequence drive the stepper motor , which can be observed Figures 18 and 19. The Figures 20 and 21 show the oscillatory behavior of the overlap of the flexible beam when applied to the second control strategy , the behavior of the flexible beam because the first sequence of actuation of the stepper motor , so as to theoretical results for the experimental results.

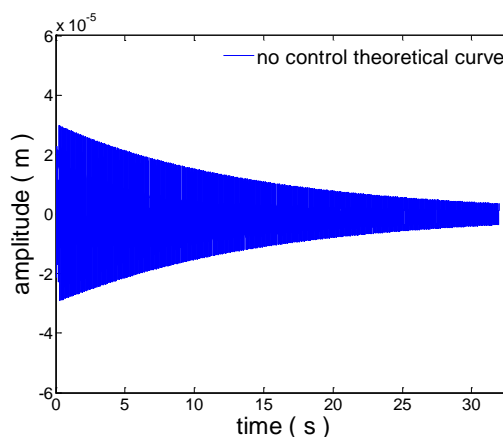


Figure 11: theoretical curve continuous drive stepper motor.

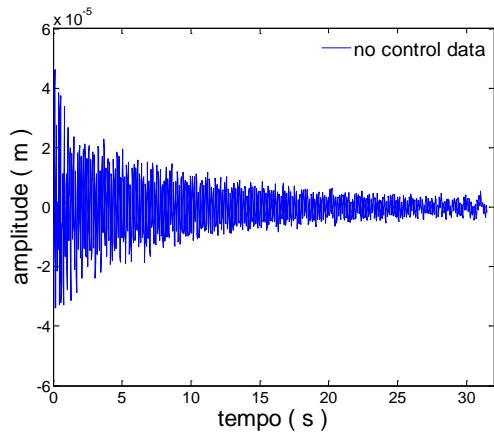


Figure 12: Experimental continuous data drive stepper motor.

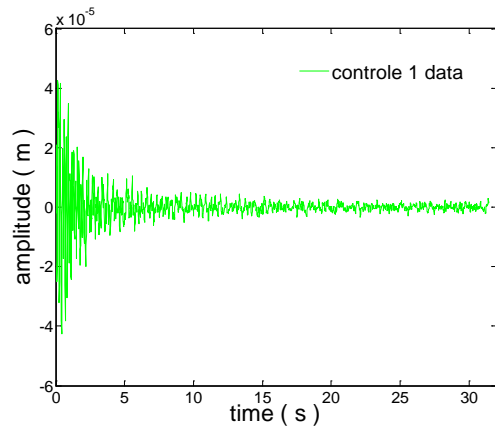


Figure 15: First control strategy experimental data.

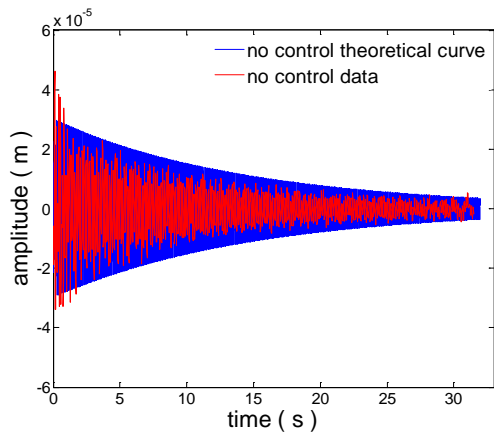


Figure 13: Superposition of the experimental and theoretical curves, drive continuous

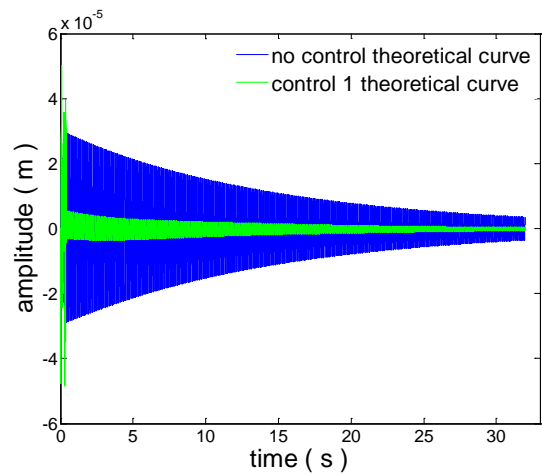


Figure 16: Theoretical curve, first control strategy and drive continuous.

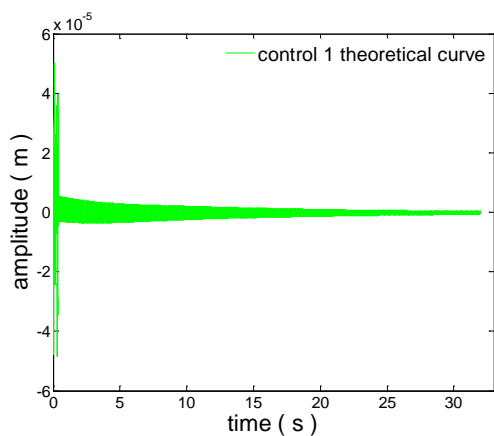


Figure 14: First control strategy, theoretical curve.

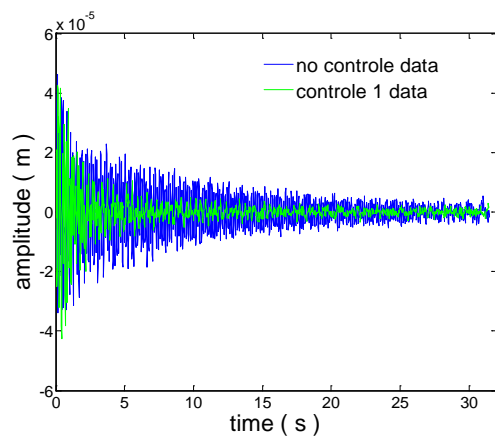


Figure 17: Experimental data, first control strategy and drive continuous.

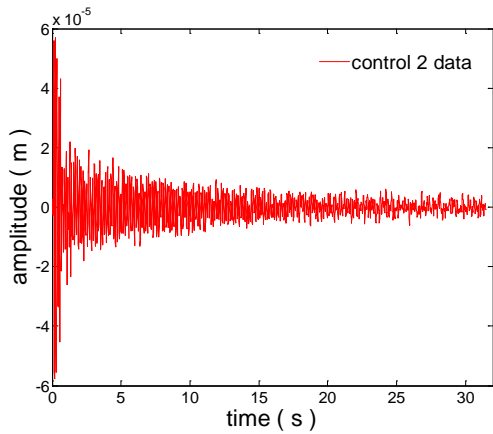


Figure 18: Deflection of the beam, second control strategy, experimental data.

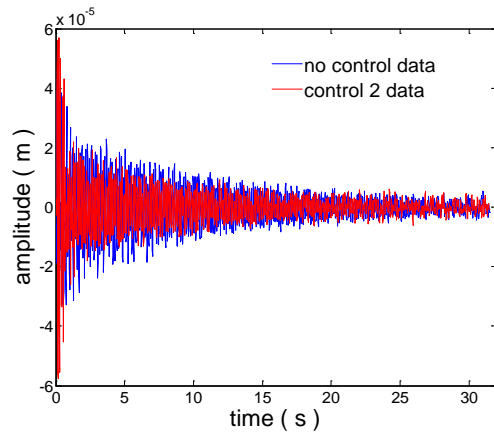


Figure 21: Experimental data, second control strategy and experimental data.

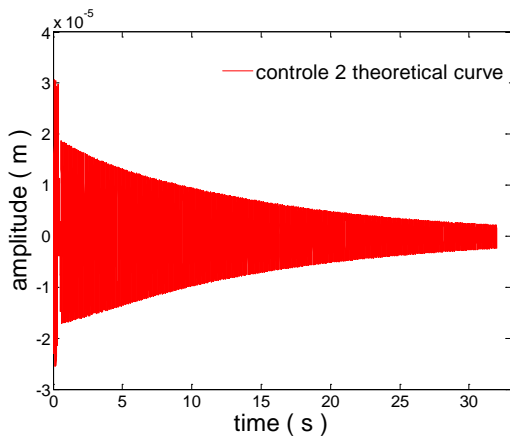


Figure 19: Deflection of the beam, second control strategy, theoretical curve.

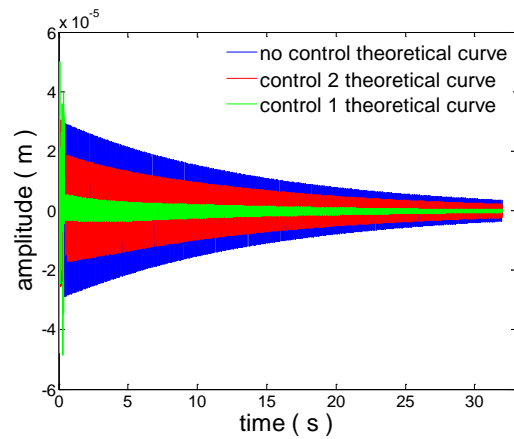


Figure 22: Deflection of the beam in the three cases drive the stepper motor, the theoretical curve.

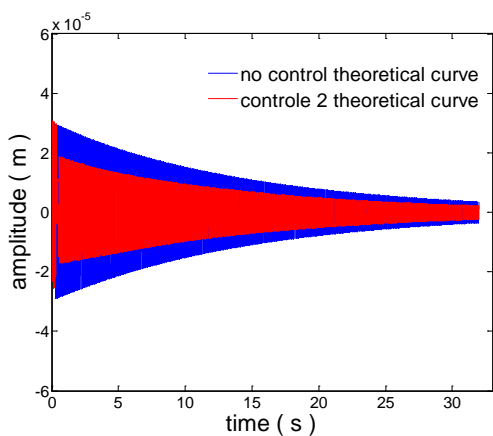


Figure 20: Superposition of the theoretical curve second control strategy and continuous drive.

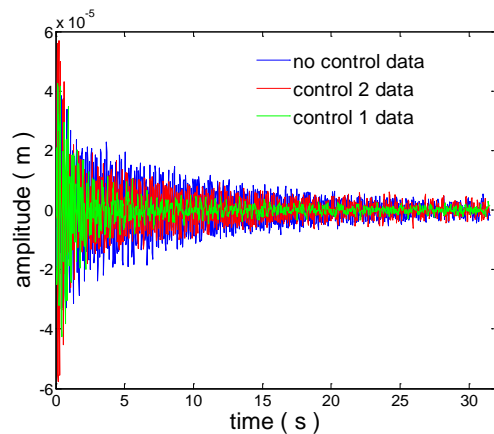


Figure 23: Deflection of the beam in the three Cases drive the stepper motor experimental data

The Figures 22 and 23 show the three cases of deflection (experimental and theoretical) due to the three sequences drives the stepper motor. The efficiency of the two design strategies vibration control can be observed. Can infer that knowing well the structure parameters for the calculation of natural frequencies, zeros can be allocated strategically about the poles of the system for maximum efficiency in reducing the amplitude of vibration of the flexible beam. However, when there are inaccuracies in the parameters of the system, the control action must be able to act to keep the displacement of the flexible beam at acceptable levels.

11 Conclusions

The vibration reduction structure using the input shaping technique, depends on proper identification of system parameters, so that the natural resonant frequency due to application of an external torque unit may be found by means of modal analysis. The use of the input shaping technique to reduce the vibration to acceptable levels in a structure that is externally excited by periodic pulses, presented good results in the neutralization of undesired vibration mode. The first control strategy, which consisted in allocating a zero on the pole of the system showed good efficiency in reducing vibration on the flexible beam. However, when inaccuracies were considered over the system parameters, two zeros were placed near the pole. The second control strategy of flexible beam, does not neutralize the influence of the pole at structure completely.

References

- [1] Tuttle, T. D.; Seering, W. P. A Zero-placement technique for designing shaped inputs to suppress multiple-mode vibration, *In: American Control Conference*, Vol.3 1994, pp 2533-2537.
- [2] Doherty, M.J. ; Tolson, R.J., Input shaping to reduce solar array structural vibrations. Hampton, Virginia: The George Washington University, Joint Institute for Advancement of Flight Sciences NASA Langley Research Center, 122p, serial number INPE-900155
- [3] Beer, F.P.; Johnston Jr., E.R. *Resistência dos materiais*. São Paulo: Itaim-Bibi, 1989.
- [4] Craig, R. R. Jr. *Structural dynamics: An Introduction to Computer Methods*. USA: John Wiley & Sons, Inc. 1981.
- [5] Ogata, K, *Discrete-time control systems*. Englewood Cliffs, NJ : Prentice-Hall, 1987.
- [6] Neri F. (2005). Cooperative evolutive concept learning: an empirical study. *WSEAS Transaction on Information Science and Applications*, WSEAS Press (Wisconsin, USA), issue 5, vol. 2, pp. 559-563.
- [7] Branco, J.; Varum, H.; Cruz, P. (2006) - Mechanical Characterization of Timber in Structural Sizes. Bending and Compression Tests - *Materials Science Forum, Trans Tech Publications, Switzerland*, ISSN 0255-5476, Vols. 514-516, May 2006, pp. 1663-1667.
- [8] Gilbert, R.C., S. Raman, T.B. Trafalis, S.M. Obeidat, and J.A. Aguirre-Cruz, Mathematical Foundations for Form Inspection and Adaptive Sampling, *Journal of Manufacturing Science and Engineering*, vol. 131, iss.4, pp. 041001, 2009
- [9] FREITAS, W. A., FENILI, A., RICCI, M.C. "Técnica de Construção de Amplitudes Impulsivas de Torque para Redução de Vibrações Residuais em uma Viga Flexível de Euler-Bernoulli. *XVI Colóquio Brasileiro de Dinâmica Orbital, XVI CBDO*, Serra Negra, S.P., 26 de novembro a 30 de novembro de 2012.
- [10] FREITAS, W. A., FENILI, A., RICCI, M.C. *XIII Colóquio Brasileiro de Dinâmica Orbital, XIII CBDO*, Bertioiga, S.P., 27 de novembro a 1 de dezembro de 2006, p.43
- [11] FREITAS, W. A., RICCI, M.C. Redução de Vibrações em Satélites Artificiais. *X Colóquio Brasileiro de Dinâmica Orbital, XII CBDO*, S.P., 20 a 25 de novembro de 2000, p.131
- [12] LI SHUANG, WANG ZHIXIN, WANG GUOQIANG A Feedback Linearization Based Control Strategy for VSC-HVDC Transmission Converters *WSEAS TRANSACTIONS on SYSTEMS*. Volume 10, 2011 Print ISSN: 1109-2777 E-ISSN: 2224-2678
- [13] Cheng-Shun Chen, Jen-Hsin Ou, Cheng-Jie Hsu Simulation Analysis of Shell Aluminum Alloy Tube For Neck-In Spinning Process *WSEAS Transactions on Systems* Print ISSN: 1109-2777 E-ISSN: 2224-2678 Volume 11, 2012
- [14] Singer, N. C and Seering, W. P. Preshaping Command Inputs to Reduce System Vibration, *ASME Journal of Dynamic Systems, Measurements, and Control*, March 1990, vol. 112, pp. 76-81.
- [15] Hyde, J. M. and Seering, W. P. Using Input Command Pre-Shaping to Suppress Multiple Mode Vibration, *Proceeding of the 1991 IEEE International Conference on Robotics and Automation*, Sacramento, CA, April 1991, pp. 2604-2609.

- [16] Murphy, B. R. and Watanable,I. Digital Shaping Filters for Reducing Machine Vibration, *IEEE Transactions on Robotcs and Automation*, April 1992, vol. 8, No. 2, pp. 285-289.
- [17] Singh, T.and Vadali, S. R. Robust Time-Delay Control, *ASME Journal of Dynamic Systems, Measurements, and Control*, March 1993, Vol. 115, pp. 303-306.
- [18] Smith, O. J. M. Feedback Control System, McGraw-Hill Book Company, Inc., New York, pp. 331-345, 1958.